CHIN. PHYS. LETT. Vol. 37, No. 9 (2020) 095201

Verification of Energetic-Particle-Induced Geodesic Acoustic Mode in Gyrokinetic Particle Simulations

Yang Chen(陈洋)[1,2,3], Wenlu Zhang(张文禄)[2,4,3,1,5*], Jian Bao(包健)[2,3], Zhihong Lin(林志宏)[6], Chao Dong(董超)[2,3], Jintao Cao(曹金涛)[2,3], and Ding Li(李定)[2,4,3,5]

[1]*School of Physical Sciences, University of Science and Technology of China, Hefei 230026, China*
[2]*Beijing National Laboratory for Condensed Matter Physics and Laboratory of Soft Matter Physics, Institute of Physics, Chinese Academy of Sciences, Beijing 100190, China*
[3]*School of Physical Sciences, University of Chinese Academy of Sciences, Beijing 100049, China*
[4]*Songshan Lake Materials Laboratory, Dongguan 523808, China*
[5]*CAS Center for Excellence in Ultra-intense Laser Science, Shanghai 201800, China*
[6]*Department of Physics and Astronomy, University of California, Irvine, California 92697, USA*

(Received 27 May 2020; accepted 7 July 2020; published online 1 September 2020)

The energetic-particle-induced geodesic acoustic mode (EGAM) is studied using gyrokinetic particle simulations in tokamak plasmas. In our simulations, exponentially growing EGAMs are excited by energetic particles with a slowing-down distribution. The frequencies of EGAMs are always below the frequencies of GAMs, which is due to the non-perturbative contribution of energetic particles (EPs). The mode structures of EGAMs are similar to the corresponding mode structures of GAMs. Our gyrokinetic simulations show that a high EP density can enhance the EGAM growth rate, due to high EP free energy, and that EPs' temperature and the pitch angle of the distribution modify the EGAM frequency/growth rate by means of the resonance condition. Kinetic effects of the thermal electrons barely change the EGAM frequency, and have a weak damping effect on the EGAM. Benchmarks between the gyrokinetic particle simulations and a local EGAM dispersion relation exhibit good agreement in terms of EGAM frequency and growth rate.

PACS: 52.35.Bj, 52.40.Mj, 52.30.−q DOI: 10.1088/0256-307X/37/9/095201

Geodesic acoustic modes[1] (GAMs) are the non-zero frequency components of zonal flow,[2−4] and have been widely observed in tokamak experiments,[5−7] investigated in theory,[8,9] and studied in simulations.[10−15] A GAM arises[16] due to the ion radial magnetic drift induced by the geodesic curvature of an equilibrium magnetic field, where magnetic drift can cause a finite radial electric field. A GAM is predominantly an electrostatic mode with a dominant $n/m = 0/0$ electrostatic potential perturbation and a dominant $n/m = 0/1$ density perturbation,[17,18] where n/m are the toroidal/poloidal mode numbers, respectively. A GAM can easily be damped by means of ion Landau damping,[19,20] and GAMs typically occur on the edges of tokamaks.[21,22] GAMs can be excited by turbulence, then regulate turbulence, and also affect turbulent transport.[7,23,24] GAMs can also be excited by the velocity space anisotropy of energetic particles (EGAM);[25] EGAMs have been theoretically predicted[25] in conditions involving slowing-down energetic particle (EP) distributions. The EGAM was first observed in a DIII–D experiment,[26] where it caused a loss of beam ions.

EPs generated where auxiliary heating, such as neutral beam injection (NBI), ion cyclotron resonance heating (ICRH), and electron cyclotron resonance heating (ECRH) exhibit a highly anisotropic distribution in velocity space.[16] An EGAM can be destabilized when the driving force of the anisotropic energetic particles exceeds the total background damping of GAM, thus the EGAM can induce the loss of energetic particles and degrade the confinement of energetic particles. As a type of energy channeling from EPs to the thermal particles, EGAMs are of key importance in terms of fusion plasmas, based on the fact that EPs can destabilize EGAMs through wave-particle resonance, while thermal ions obtain energy from the EGAM through Landau damping.

EGAMs have also been observed in the large helical device (LHD)[27] with NBI, in JET[28,29] with ICRH, in ASDEX-Upgrade[30] with NBI, in HL-2A[31] with ECRH, and recently in EAST[32] with NBI. Several theories have been developed to investigate EGAM, including excitation due to the sharp gradient in a pitch angle,[33] local and global EGAM disper-

Supported by the National MCF Energy R&D Program (Grant Nos. 2018YFE0304100, 2018YFE0311300 and 2017YFE0301300), the National Natural Science Foundation of China (Grant Nos. 11675256, 11675257, 11835016, 11875067 and 11705275), the Strategic Priority Research Program of the Chinese Academy of Sciences (Grant No. XDB16010300), the Key Research Program of Frontier Science of the Chinese Academy of Sciences (Grant No. QYZDJ-SSW-SYS016), and the External Cooperation Program of the Chinese Academy of Sciences (Grant No. 112111KYSB20160039).
*Corresponding author. Email: wzhang@iphy.ac.cn
© 2020 Chinese Physical Society and IOP Publishing Ltd

sion relation,[34] nonlinear second harmonics,[35] energy channeling,[36] excitation using not fully slowed-down EPs,[17] the finite β effect on mode structure,[37] and the dispersion relation of the EGAM with a bump-on-tail EPs distribution.[38] Simulations based on LHD equilibrium and its parameters have been carried out to investigate EGAMs in terms of its linear property,[39] high-frequency branch,[40] and energy channeling.[41] A gyro-kinetic simulation[42] investigated the impact of EGAM on turbulent transport.

Although many works relating to EGAMs have been performed, both experimentally and theoretically, nonlinear simulations in this area have been far from adequate. As a rehearsal for a future nonlinear EGAM simulation, in this work, we use the gyrokinetic toroidal code (GTC)[3] to investigate the linear excitation of the local EGAM, and to verify the EGAM by benchmarking, using theoretical works, via quantitative analysis. The GTC has been successfully applied to study GAMs,[10,15] turbulence,[24,43,44] and MHD instabilities induced by energetic particles such as fast-ion-driven toroidal Alfvén eigenmodes (TAEs),[45,46] as well as energetic-electron-driven β-induced Alfvén eigenmodes (e-BAE).[47,48]

In our simulations, the thermal ions are described by nonlinear gyrokinetic equations.[49] The thermal electrons are described by an electrostatic version of the fluid-kinetic hybrid model,[50–52] in which the electrons' response is expanded into a lowest-order adiabatic element and a high-order non-adiabatic kinetic perturbation element.

The anisotropic slowing-down distribution function for energetic particles used in this work is expressed as follows:

$$f_{0\alpha} = c\frac{n_{0\alpha}(\psi)H(v_0 - v)}{v^3 + v_c^3}\exp\left[-\left(\frac{\Lambda - \Lambda_0}{\Delta\Lambda}\right)^2\right], \quad (1)$$

where $f_{0\alpha}$ is the gyrocenter distribution function, $v = \sqrt{v_\parallel^2 + 2\mu B_0/m_\alpha}$, $v_\parallel$ is the parallel velocity, μ is the magnetic moment, m_α is the mass of the energetic particles, B_0 is the equilibrium magnetic field, v_c is critical velocity,[53] v_0 is the birth speed, H is the Heaviside step function, c is the normalization factor, and $n_{0\alpha}$ is the density of EPs. Here, $\Lambda \equiv \mu B_a/E$ denotes the pitch angle, E is the energetic particles' kinetic energy, B_a is the on-axis magnetic field, Λ_0 is the peak of the pitch angle, and $\Delta\Lambda$ is the width of the pitch angle.

The energetic particles are described by the general weight equation, which can be derived from the gyrokinetic equations by holding μ constant:

$$\begin{aligned}\frac{dw_\alpha}{dt} =& (1 - w_\alpha)\left[-\left(v_\parallel\frac{\delta\boldsymbol{B}}{B_0} + v_E\right)\cdot\left(\frac{1}{n_{0\alpha}}\frac{\partial n_{0\alpha}}{\partial\psi}\nabla\psi\right)\right.\\ &+ (Z_\alpha\boldsymbol{v}_d\cdot\nabla\delta\phi - Z_\alpha v_\parallel E_\parallel)\\ &\left.\times\left(\frac{2\Lambda^2}{B_\alpha\Delta\Lambda^2}(\Lambda - \Lambda_0) - \frac{1}{m_\alpha}\frac{3\mu v}{v^3 + v_c^3}\right)\right], \quad (2)\end{aligned}$$

where the particle weight is defined as $w_\alpha \equiv \delta f_\alpha/f_\alpha$, with δf_α being the perturbed distribution and f_α being the total distribution; $\delta\phi$ is the perturbed electrostatic potential, $\delta\boldsymbol{B}$ is the perturbed magnetic field, and $E_\parallel = -(\boldsymbol{B}_0/B_0)\cdot\nabla\delta\phi$ is the parallel electric field. Here $\boldsymbol{v}_E$ is the $\boldsymbol{E}\times\boldsymbol{B}$ drift velocity, $\boldsymbol{v}_d$ is the magnetic drift velocity, ψ is the poloidal flux label, and Z_α is the EPs' charge. Note that $\delta\boldsymbol{B} = 0$ in the above weight equation for this electrostatic simulation. The system can be closed via gyrokinetic Poisson equations.[49]

The simulation results are obtained under the following equilibrium and parameters: the major radius is $R_0 = 170\,\mathrm{cm}$. The inverse aspect ratio is $\epsilon \equiv a/R_0 = 0.3$ in a tokamak with a concentric circular cross section, where a is the tokamak minor radius. The magnetic field amplitude on the magnetic axis is $B_0 = 2\,\mathrm{T}$. The background plasma is uniform, with the temperature of the thermal ions and the thermal electrons being $T_e = T_i = 1000\,\mathrm{eV}$. The thermal electron density is $n_e = 7.9\times10^{13}\,\mathrm{cm}^{-3}$. The background thermal ions and the energetic particles are protons. The thermal ion density can be obtained from the quasi-neutral condition $Z_i n_i + Z_b n_b = n_e$, where n_b is the density of the energetic particles, and where $Z_i = Z_b = 1$ for protons. We use a constant $q = 4$ profile for simplicity, since magnetic shear has little effect on the GAM's frequency and damping rate. Our simulation domain in the radial direction is $0.2 \leqslant \rho \leqslant 0.8$, where $\rho = \sqrt{\psi_p/\psi_{pw}}$ is the square root of the normalized poloidal flux, ψ_p is the poloidal flux, and ψ_{pw} is the poloidal flux at the edge. A toroidal/poloidal filter is adopted to preserve only the $n/m = 0/(0,1,2)$ harmonics, so as to avoid high-frequency noise. The numerical parameters have been carefully chosen based on convergence tests. The time step is $\Delta t = 0.02R_0/C_s$, where $C_s = \sqrt{T_e/m_i}$ is the sound speed. In this work, there are 140 radial grid points, 1320 poloidal grid points, and 32 toroidal grid points in the real space, making sure that the grid size is on the same order as the thermal ions' gyroradius in order to obtain better simulation properties in particle-in-cell simulations. There are 100 marked particles in each grid cell.

We first initialize a flux-surface-averaged ion density perturbation in order to generate the GAM. In the radial direction, the density perturbation is set to be a sine function, and its value is set to be zero at the boundaries. The initial density perturbation can induce an electrostatic field perturbation. The time evolution of the perturbed electrostatic potential $\delta\phi$ is as shown in Fig. 1(a). The GAM decays exponentially during the initial perturbation, with the real frequency $\omega = 1.03\omega_G$, which is slightly higher than the GAM frequency, where $\omega_G = \sqrt{(\frac{7}{2}T_i + 2T_e)/(m_i R_0^2)}$ is the leading order of the local GAM frequency.[34] The poloidal mode structure of the perturbed electrostatic potential is shown in Fig. 1(b), the corresponding ra-

dial profile is shown in Fig. 1(c), and the dominant mode number is $n/m = 0/0$. The poloidal mode structure of the perturbed density is shown in Fig. 1(d), the corresponding radial profile is shown in Fig. 1(e), and the dominant mode number is $n/m = 0/1$. The poloidal mode structure and radial profile of the perturbed electrostatic potential and the perturbed density are plotted at the same time $t = 10R_0/C_s$. The mode number and mode frequency are consistent with the GAM's basic property.

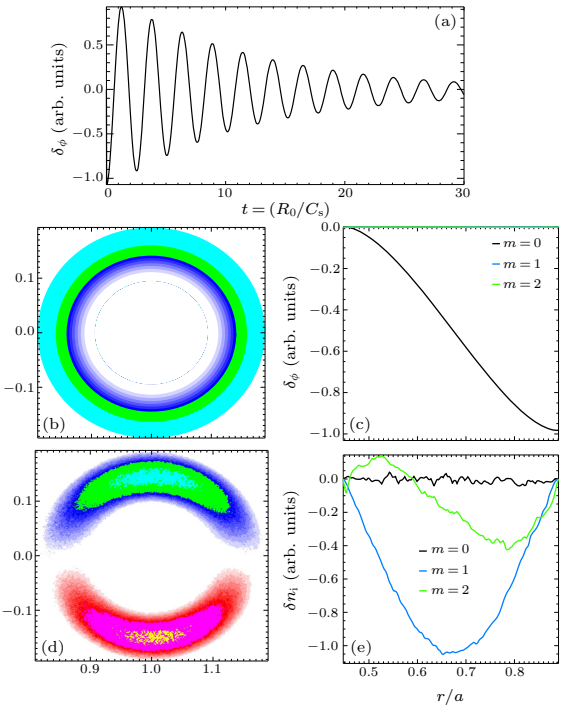

Fig. 1. (a) Time history of the electrostatic potential $\delta\phi$ for GAM with an initial perturbation. [(b),(d)] Poloidal mode structures of the perturbed electrostatic potential $\delta\phi$, and the perturbed density δn_i. [(c),(e)] Radial profiles of the corresponding perturbed electrostatic potential $\delta\phi$, and the perturbed density δn_i for the main harmonic and other harmonics, normalized with respect to the maximum value of their own amplitude.

Next, we use anisotropic energetic particles to excite the EGAM. In velocity space, a typical energetic particle distribution is shown in Eq. (1) and the corresponding parameters are set as follows: the pitch angle peak is set to $\Lambda_0 = 0.5$, the pitch angle width is set to $\Delta\Lambda = 0.05$, and the birth speed is set to $v_0 = 1.2q\omega_G R_0$. In this case, the transit frequency of energetic particles $\omega_{tr,b} \equiv v_\parallel/(qR)$ is close to ω_G, which makes it easy for energetic particles to induce an EGAM through wave-particle resonance. The critical velocity v_c is a constant associated with the temperature of the thermal electrons. A typical energetic particle's density profile in spatial space is expressed as $n_b = 0.08\{1.0 + 0.2[\tanh(0.5 - \rho)/0.03] - 1\}n_e$. We define the equivalent temperature of energetic particles with a slowing-down distribution as $T_{\alpha s}$, which can be expressed as $T_{\alpha s} = (2I_4)/(3I_2)E_b$,[54] where $E_b = 1/2m_\alpha v_0^2$ is the birth energy, and $I_n(a) = \int_0^1 x^n/(a^3 + x^3)dx$. In the above EP setup, the equivalent temperature in our simulations is $T_{\alpha s} \sim 0.274E_b \sim 40.8T_e$. In these simulation scenarios, the EGAM grows exponentially in linear simulations. The time evolution of the perturbed electrostatic potential $\delta\phi$ is shown in Fig. 2(a), where the x-axis is normalized with respect to R_0/C_s, and the y-axis is normalized by a maximum of $\delta\phi$ at $t = 40R_0/C_s$. The EGAM frequency is $\omega = 0.544\omega_G$, with a growth rate of $\gamma = 0.240\omega_G$. The EGAM frequency is about half the GAM frequency under the same equilibrium and simulation parameters, which means that a non-perturbative contribution by energetic particles can induce an EGAM and modify the frequency. The poloidal mode structure of the perturbed electrostatic potential for the EGAM is shown in Fig. 2(b), the corresponding radial profile is shown in Fig. 2(c), and the dominant mode number is $n/m = 0/0$. The mode structure is not affected by energetic particles. The poloidal mode structure of the perturbed density is shown in Fig. 2(d), the corresponding radial profile is shown in Fig. 2(e), and the dominant mode number is $n/m = 0/1$.

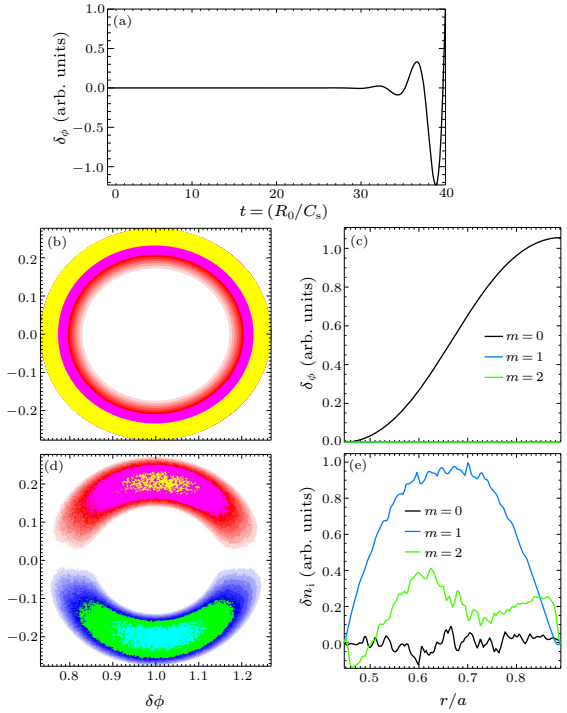

Fig. 2. (a) Time history of electrostatic potential $\delta\phi$ for the EGAM. [(b),(d)] Poloidal mode structures of the electrostatic potential $\delta\phi$, and the perturbed density δn_i. [(c),(e)] Radial profiles of the corresponding electrostatic potential $\delta\phi$, and the perturbed density δn_i for the main harmonic and other harmonics, normalized with respect to the maximum value of their own amplitude.

Since this work is the first gyrokinetic particle simulation of the EGAM in GTC, we verify the EGAM simulations by benchmarking with a local EGAM theory.[34] In local EGAM theory, the thermal ions and

energetic particles are described by gyrokinetic equations, and the finite electron Larmor radius effects are ignored. The physical model used in our simulations is similar to the physical model used in the theoretical work. The mean optimal ordering adopted to derive the dispersion relation in the theoretical publication is as follows:

$$\frac{1}{q} \sim O(\delta^{1/2}), \quad \omega_{\mathrm{tr,b}} \sim \omega, \quad \frac{n_{\mathrm{b}}}{n_{\mathrm{e}}} \sim O(\delta).$$

The simulation parameters are carefully set to match the optimal ordering. We use a finite pitch angle width slowing-down distribution to approach the single pitch angle slowing-down distribution used in theory, and convergence tests are then conducted.

The local EGAM dispersion relation[34] can be given as follows:

$$-1+\frac{\omega_{\mathrm{G}}^2(r)}{\omega^2}+N_{\mathrm{b}}(r)\left[C\ln\left(1-\frac{\omega_{\mathrm{tr,b}}^2}{\omega^2}\right)\right.$$
$$\left.+\frac{\Lambda_0 B(2-\Lambda_0 B)^2}{(1-\Lambda_0 B)^{5/2}}\frac{\omega_{\mathrm{tr,b}}^2/\omega^2}{1-\omega_{\mathrm{tr,b}}^2/\omega^2}\right]=0, \qquad (3)$$

where $C = [(2-\Lambda_0 B)(-2+5\Lambda_0 B)]/[2(1-\Lambda_0 B)^{5/2}]$ is a constant associated with the pitch angle peak, $\omega_{\mathrm{tr,b}} = \sqrt{2E_{\mathrm{b}}(1-\Lambda_0 B)}/(qR)$ is the transit frequency of energetic particles, $N_{\mathrm{b}}(r) = [\sqrt{1-\Lambda_0 B}q^2 n_{\mathrm{b}}]/[4n_{\mathrm{c}}\ln(E_{\mathrm{b}}/E_{\mathrm{c}})]$ is the density perturbation term, and E_{b} and E_{c} denote the birth energy and the critical energy, respectively.

To numerically solve the dispersion relation (3), we present the following analysis. We set $X = \omega_{\mathrm{tr,b}}^2/\omega^2$ as a variable, where X is a complex number. The dispersion relation can be simplified to

$$1-X = \exp\left[A - BX - \frac{DX}{1-X}\right],$$

where A, B, and D are the real constants associated with the simulation parameters. By separating the complex equation into a real part and an imaginary part, we obtain the equations which can be solved numerically. These equations have several solutions in the whole region; however, by taking the frequency and the growth rate of our simulation results as a trial solution, the numerical solution of the dispersion relation is $\omega = 0.571\omega_{\mathrm{G}}$, and the corresponding growth rate is $\gamma = 0.214\omega_{\mathrm{G}}$. Our simulation results show good agreement in terms of EGAM frequency and growth rate with the local EGAM dispersion relation. The numerical error is within 12%, which may be ascribed to the large aspect ratio used in the theory.

Several simulations have also been conducted to investigate the properties of the EGAM, and to compare them with theoretical works via quantitative analysis.

We define $Z = v_0/(qR_0\omega_{\mathrm{G}})$ as a function of the birth speed. As shown in Fig. 3(a), in simulations, the mode frequency increases with the increasing Z value, while the growth rate firstly increases and then decreases with the increasing Z value. Generally speaking, the wave-particle resonance condition[55] for purely passing particles is $\omega - k_{\parallel}v_{\parallel} - p\omega_{\mathrm{tr}} = 0$, where p is an integer number. With regard to the EGAM, $k_{\parallel} \equiv (nq-m)/Rq = 0$, so the resonance condition can be written as $\omega - p\omega_{\mathrm{tr}} = 0$. Further analysis reveals that the primary ($p = 1$) transit resonance is the most important.[16] This explains the trend in the growth rate: the transit resonance between energetic particles and the EGAM is weakened when the birth speed exceeds the transit speed by too great an extent. The corresponding numerical solutions of the theoretical dispersion relation are also plotted in Fig. 3(a). The mode frequency and the growth rate increases with an increase in the value of Z.

A similar Z scan has been carried out where the density of energetic particles is set to $n_{\mathrm{b}} = 0.065n_{\mathrm{e}}$. As shown in Fig. 3(b), our simulation results agree well with the theoretical prediction in terms of both frequency and growth rate. The real frequencies of EGAMs are always below the real frequencies of GAMs across a wide range of parameters under the same simulation conditions, with the exception of EPs.

In the above Z scans, the discrepancy in the growth rate between the simulations and the theory is due to the fact that the optimal ordering used in the theory is broken at large Z values, so that the dispersion relation may not be sufficiently accurate.

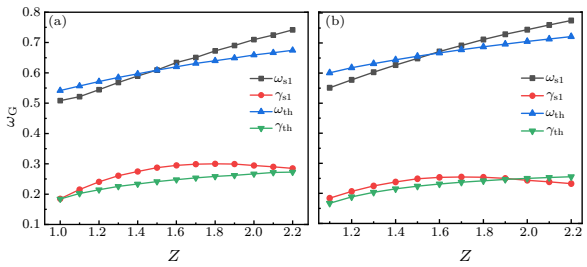

Fig. 3. Z Scan of EGAM frequency and linear growth rate where the energetic particle density is (a) $n_{\mathrm{b}} = 0.08n_{\mathrm{e}}$, and (b) $n_{\mathrm{b}} = 0.065n_{\mathrm{e}}$.

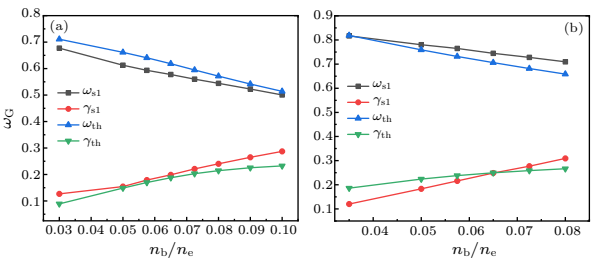

Fig. 4. Energetic particle density n_{b} scan of EGAM frequency and linear growth rate when (a) $Z = 1.2$ and (b) $Z = 2$.

Two unstable branches of EGAMs can be predicted in the theory: the GAM branch, where $\omega_{\mathrm{G}} < \omega_{\mathrm{tr,b}}$, and the Beam branch, where $\omega_{\mathrm{G}} > \omega_{\mathrm{tr,b}}$. We select $Z = 1.2$ (beam branch) as shown in Fig. 4(a), and

$Z = 2$ (GAM branch) as shown in Fig. 4(b) in order to investigate the influence of EP density on the real frequency and the corresponding growth rate for different branches. As shown in Fig. 4, as the density of EPs increases, the frequency decreases considerably, and the growth rate increases considerably. In both branches, the simulation results agree with the theory very well in relation to both frequency and growth rate.

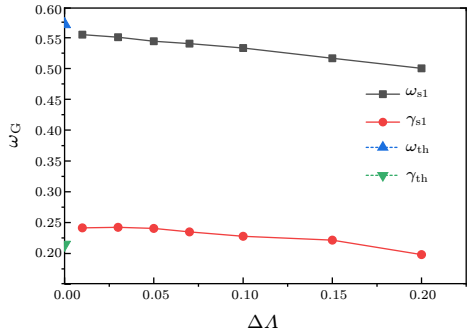

Fig. 5. Pitch angle width $\Delta\Lambda$ scan of EGAM frequency and linear growth rate when $Z = 1.2$ and $n_b = 0.08n_e$. The signals (up-triangle and down-triangle) are the frequency and the growth rate of the theoretical prediction (we take $\Delta\Lambda$ as approaching zero to represent the single pitch angle distribution used in the theoretical work).

Since we use a finite pitch angle width, $\Delta\Lambda = 0.05$, to approach the single pitch angle assumption used in the theory, a pitch angle width scan is also performed. As shown in Fig. 5, as the pitch angle width $\Delta\Lambda$ decreases, the real frequency increases, and the corresponding growth rate increases. Both the frequency and the growth rate gradually approach a stable value as $\Delta\Lambda$ decreases gradually to zero, and there is little difference in the real frequency and growth rate when the pitch angle width, $\Delta\Lambda$, is sufficiently small. Our simulation results are consistent with the theoretical prediction where the pitch angle width is sufficiently small.

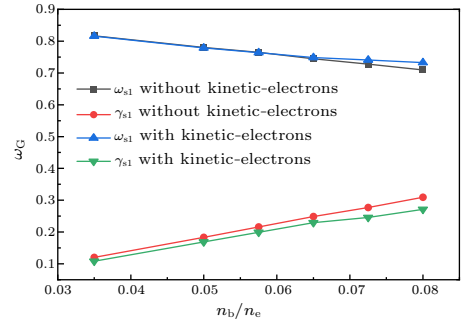

Fig. 6. Energetic particle density n_b scan of EGAM frequency and linear growth rate with/without the kinetic effects of thermal electrons, where $Z = 2$.

As shown in Fig. 6, the EGAM frequency barely changes, and the corresponding growth rate is lower in simulations with kinetic electrons, indicating that the kinetic effects of thermal electrons have a weakly damping effect on the excitation of the EGAM. This collisionless damping can be ascribed to the kinetic effects of the trapped thermal electrons via the bounce resonance with EGAMs.[10]

In summary, the gyrokinetic toroidal code (GTC) has been successfully employed to study EGAMs in toroidal plasmas. In our simulations, energetic particles with a slowing-down distribution can drive EGAMs through wave-particle transit resonance. The mode structures of EGAMs are not affected by EPs. The non-perturbative contributions of energetic particles reduce the mode frequency and modify the growth rate. With an increase in the birth speed of EPs, the EGAM frequency increases, and the growth rate firstly increases and then decreases, which is due to the detuning of EPs and EGAMs. With an increase in the EP density, the EGAM frequency decreases, and the growth rate increases. As the pitch angle width gradually decreases to zero, both the EGAM frequency and the corresponding growth rate increase gradually to a constant value, and there is little difference in either frequency or growth rate when the pitch angle width $\Delta\Lambda$ is sufficiently small. Kinetic electrons have a slight inhibitory effect on the excitation of EGAMs. Benchmarks between gyrokinetic particle simulations and local EGAM dispersion relation show good agreement in terms of both the real frequency and growth rate of EGAMs.

The authors wish to thank Dr. Zhi-Yong Qiu, S. Taimourzadeh, W. Hu, and Z. Ge for useful discussions. This research employed the resources of the National Supercomputer Center in Tianjin (NSCC-TJ), the Oak Ridge Leadership Computing Facility at Oak Ridge National Laboratory (OLCF) and the National Energy Research Scientific Computing Center (NERSC).

References

[1] Winsor N, Johnson J L and Dawson J M 1968 *Phys. Fluids* **11** 2448
[2] Hasegawa A, Maclennan C G and Kodama Y 1979 *Phys. Fluids* **22** 2122
[3] Lin Z, Hahm T S, Lee W W, Tang W M and White R B 1998 *Science* **281** 1835
[4] Wang G, Ma J, Weiland J and Zagorodny A G 2015 *Chin. Phys. Lett.* **32** 115201
[5] Hamada Y, Nishizawa A, Ido T, Watari T, Kojima M, Kawasumi Y, Narihara K, Toi K and Group J I 2005 *Nucl. Fusion* **45** 81
[6] Lan T, Liu A D, Yu C X, Yan L W, Hong W Y, Zhao K J, Dong J Q, Qian J P, Cheng J, Yu D L *et al.* 2008 *Phys. Plasmas* **15** 056105
[7] Hasegawa A and Wakatani M 1987 *Phys. Rev. Lett.* **59** 1581
[8] Gao Z 2013 *Phys. Plasmas* **20** 032501
[9] Chakrabarti N, Singh R, Kaw P K and Guzdar P N 2007 *Phys. Plasmas* **14** 052308
[10] Zhang H S and Lin Z 2010 *Phys. Plasmas* **17** 072502
[11] Xu X Q, Xiong Z, Gao Z, Nevins W M and Mckee G R 2008 *Phys. Rev. Lett.* **100** 215001
[12] Zarzoso D, Garbet X, Sarazin Y, Dumont R and Grandgirard V 2012 *Phys. Plasmas* **19** 022102
[13] Wang H, Todo Y and Kim C C 2013 *Phys. Rev. Lett.* **110**

155006
[14] Dorf M, Cohen R H, Dorr M R, Rognlien T D, Hittinger J A, Compton J C, Colella P, Martin D F and Mccorquodale P 2013 *Nucl. Fusion* **53** 063015
[15] Zhang H, Qiu Z, Chen L and Lin Z 2009 *Nucl. Fusion* **49** 125009
[16] Zhiyong Q, Zonca F and Liu C 2011 *Plasma Sci. Technol.* **13** 257
[17] Cao J, Qiu Z and Zonca F 2015 *Phys. Plasmas* **22** 124505
[18] Guo W F, Wang S J and Li J G 2009 *Chin. Phys. Lett.* **26** 045202
[19] Lebedev V B, Yushmanov P N, Diamond P H, Novakovskii S V and Smolyakov A I 1996 *Phys. Plasmas* **3** 3023
[20] Novakovskii S V, Liu C S, Sagdeev R Z and Rosenbluth M N 1997 *Phys. Plasmas* **4** 4272
[21] Qiu Z, Chen L and Zonca F 2009 *Plasma Phys. Control. Fusion* **51** 012001
[22] Bingren S, Jiquan L I and Jiaqi D 2005 *Chin. Phys. Lett.* **22** 1179
[23] Hinton F L and Rosenbluth M N 1999 *Plasma Phys. Control. Fusion* **41** A653
[24] Liu F, Lin Z, Dong J Q and Zhao K J 2010 *Phys. Plasmas* **17** 112318
[25] Fu G Y 2008 *Phys. Rev. Lett.* **101** 185002
[26] Nazikian R, Fu G Y, Austin M E, Berk H L, Budny R V, Gorelenkov N N, Heidbrink W W, Holcomb C T, Kramer G J *et al.* 2008 *Phys. Rev. Lett.* **101** 185001
[27] Ido T, Shimizu A, Nishiura M, Nakamura S, Kato S, Nakano H, Yoshimura Y, Toi K *et al.* 2011 *Nucl. Fusion* **51** 073046
[28] Boswell C, Berk H L, Borba D, Johnson T, Pinches S D and Sharapov S E 2006 *Phys. Lett. A* **358** 154
[29] Berk H L, Boswell C, Borba D, Figueiredo A C A, Johnson T, Nave M F F, Pinches S D, Sharapov S E and Contributors J E 2006 *Nucl. Fusion* **46** S888
[30] Horvath L, Papp G, Pokol G I, Lauber P, Gabor P, Gude A and Igochine V 2016 *Nucl. Fusion* **56** 112003
[31] Chen W, Ding X T, Yu L M, Ji X Q, Shi Z B, Zhang Y P, Zhong W L, Yuan G L, Dong J Q *et al.* 2013 *Nucl. Fusion* **53** 113010
[32] Xu M, Zhang J, Zhou T, Duan Y M, Hu L, Li Y, Xu L, Shi T H, Liu Y *et al.* 2018 *Nucl. Fusion* **58** 096004
[33] Berk H L and Zhou T 2010 *Nucl. Fusion* **50** 035007
[34] Qiu Z, Zonca F and Chen L 2010 *Plasma Phys. Control. Fusion* **52** 095003
[35] Fu G Y 2011 *J. Plasma Phys.* **77** 457
[36] Sasaki M, Itoh K and Itoh S 2011 *Plasma Phys. Control. Fusion* **53** 085017
[37] Kolesnichenko Y I, Lepiavko B S and Lutsenko V V 2013 *Plasma Phys. Control. Fusion* **55** 125007
[38] Ren H and Wang H 2018 *Nucl. Fusion* **58** 046005
[39] Wang H and Todo Y 2013 *Phys. Plasmas* **20** 012506
[40] Wang H, Todo Y, Ido T and Osakabe M 2015 *Phys. Plasmas* **22** 092507
[41] Wang H, Todo Y, Oasakabe M, Ido T and Suzuki Y 2019 *Nucl. Fusion* **59** 096041
[42] Zarzoso D, Sarazin Y, Garbet X, Dumont R, Strugarek A, Abiteboul J, Cartiermichaud T, Dif-Pradalier G, Ghendrih P, Grandgirard V *et al.* 2013 *Phys. Rev. Lett.* **110** 125002
[43] Hu W, Feng H and Dong C 2018 *Chin. Phys. Lett.* **35** 105201
[44] Hu W, Feng H and Zhang W 2019 *Chin. Phys. Lett.* **36** 085201
[45] Zhang W, Holod I, Lin Z and Xiao Y 2012 *Phys. Plasmas* **19** 022507
[46] Wang Z, Lin Z, Holod I, Heidbrink W W, Tobias B, Zeeland M V and Austin M E 2013 *Phys. Rev. Lett.* **111** 145003
[47] Chen Y, Zhang W, Cheng J, Lin Z, Dong C and Li D 2019 *Phys. Plasmas* **26** 102507
[48] Cheng J, Zhang W, Lin Z, Ding L, Chao D and Cao J 2017 *Phys. Plasmas* **24** 092516
[49] Holod I, Zhang W L, Xiao Y and Lin Z 2009 *Phys. Plasmas* **16** 122307
[50] Lin Z and Chen L 2001 *Phys. Plasmas* **8** 1447
[51] Lin Z, Nishimura Y, Xiao Y, Holod I, Zhang W and Chen L 2007 *Plasma Phys. Control. Fusion* **49** B163
[52] Xiao Y, Holod I, Wang Z, Lin Z and Zhang T 2015 *Phys. Plasmas* **22** 022516
[53] Gaffey J D 1976 *J. Plasma Phys.* **16** 149
[54] Estradamila C, Candy J and Waltz R E 2006 *Phys. Plasmas* **13** 112303
[55] Chen L 1999 *J. Geophys. Res.* **104** 2421